ARCHIVES
of
FOUNDRY ENGINEERING

ISSN (2299-2944)

10.24425/afe.2025.155356

Published quarterly as the organ of the Foundry Commission of the Polish Academy of Sciences

Establishment of Heat Balance Equation and Baking Efficiency Analysis of Heat Storage Steel Ladle Baking System Based on Different Gases

Xiang Bai, Jia yang He, Hujun Mao *, Guang qiang Liu
University of Science and Technology Liaoning, School of Civil Engineering, China
* Corresponding author: E-mail address: maohj@ustl.edu.cn

Received 21.01.2025; accepted in revised form 10.03.2025; available online 23.07.2025

Abstract

The establishment of the heat balance within the ladle baking system holds paramount significance for optimizing the baking process, enhancing the quality of molten steel, and minimizing energy consumption. In this research endeavor, a meticulous mathematical model of the ladle baking system has been formulated, leveraging CFD numerical simulation and utilizing a 130-ton ladle as the benchmark prototype. The precision of this numerical simulation has been rigorously validated through experimental data. Furthermore, the formulation of the heat balance equation for the thermal storage ladle baking system has been accomplished through a harmonious blend of theoretical analysis and experimental exploration. The comparison of the energy-saving efficacy of the thermal storage ladle baker across various gas types, with a keen emphasis on analyzing ladle lining and shell volume heat storage, sheds light on the baking efficiency associated with different gas types. The study's revelations underscore that external flue gas sensible heat loss constitutes the most prominent factor, whereas ladle shell volume heat storage is the least substantial, accounting for less than 1% of the total heat involved. The chemical heat and surface heat dissipation of the gas escaping from the gap are both less than 5%; The sensible heat loss rates of gas escaping from gaps during the baking of natural gas, coke oven gas, and converter gas are 8.16%, 13.33%, and 23.96%, respectively; The radiation heat loss rates are 8.35%, 8.68%, and 14.62%, respectively; The average thermal efficiencies are 27.78%, 27.83%, and 23.80%, respectively.The findings of this research study have significantly propelled the domain of heat storage ladle baking technology to new heights. They not only contribute to the progression of ladle baking technology but also specifically enrich the understanding within the realm of thermal storage systems.

Keywords: Thermal storage steel ladle baking, Heat balance equation, Combustion efficiency, Artificial gas

1. Introduction

The regenerative ladle mainly works based on regenerative combustion technology. Generally, two regenerative burners operate alternately. When one burner is burning, the other is exhausting smoke. The high-temperature flue gas generated by combustion is discharged through the regenerative body of the exhaust burner. In this process, the flue gas exchanges heat with the regenerative body, causing the flue gas temperature to drop significantly and then be discharged by the induced draft fan. After a certain period of time, the reversing valve acts and the states of the two burners are exchanged. The burner that originally exhausted smoke turns into a burning state. Combustion-supporting air enters the regenerator and is heated, and then mixes with fuel

while burning, bringing heat back into the ladle. Through this continuous circulation way, the regenerative ladle realizes efficient recovery of waste heat from flue gas, reduces exhaust heat loss, and further improves combustion heating efficiency, achieving purposes such as energy saving and improving baking quality.

The heat balance equation for thermal storage steel ladle baking helps calculate the heat flow in and out of the system accurately. This allows us to pinpoint key heat losses, like heat escaping from the furnace and heat carried away by exhaust gases. With this understanding, we can take targeted steps to save energy and cut production costs, as shown in studies [1-3]. Additionally, this equation is crucial for ensuring the quality of ladle baking. It helps determine the best heat supply settings to optimize the ladle lining's performance and lifespan. From a system optimization angle, the heat balance equation offers a theoretical foundation for enhancing and upgrading the system. By examining the heat balance, we can adjust key components like burners and heat accumulators to boost the baking system's efficiency and stability, as highlighted in research [4, 5].

The combustion thermal efficiency stands as a crucial measure of the baking effect, offering a scientific foundation for delving into issues within the ladle baking process and assessing its quality. The assessment of the steel ladle baking effect hinges on two paramount parameters: temperature and heat storage. An elevation in temperature signifies that the steel ladle possesses greater heat retention capabilities during the baking process, ultimately elevating its overall quality [6]. While the baking temperature of the ladle can be readily measured with instrumentation, determining its heat storage necessitates meticulous data calculation. Hence, minimizing heat loss and optimizing baking efficiency have emerged as pressing concerns.

In practice, the gas type employed for ladle baking often differs due to the variety of on-site gas sources available. WEBER, R. [7, 8] and their team conducted a comprehensive study involving three fuel types: natural gas (NG), light fuel oil (LFO), and heavy fuel oil (HFO), in an experimental furnace with a heat input of 0.58MW. Their findings revealed that the temperature and concentration fields generated by these three fuels exhibited distinct behaviors. WEIHONG Y [9] conducted a comparative analysis of the ignition process of natural gas and propane under various high-temperature oxidizers. Their investigation delved into the chemistry of ignition delay time, revealing that propane has a higher propensity for ignition compared to natural gas. This finding offers valuable theoretical backing for the selection of fuels in ladle baking applications. LILLE S. [10] conducted a thorough examination of the combustion outcomes of propane fuels and numerical simulations of heat transfer within the HTAC test furnace, with a particular emphasis on pertinent stove operation issues, the high-cycle thermal regenerative combustor, the process involved, and the type of fuel utilized. The study by S á NCHEZ M. et al. [11] using coke oven gas as fuel showed that the use of artificial gas flameless combustion in self storage burners has significant advantages.

In the realm of regenerative ladle baking, it is patently evident that a thorough comparative analysis of the impacts exerted by different gases holds immense significance. This analysis serves as a linchpin for optimizing the baking process of regenerative ladles and pinpointing equivalent gas substitutes during real world baking operations. However, a conspicuous void exists in the form of systematic research on comparing the effects of various gases in the baking of thermal - storage ladles. What sets the current study apart is its innovative approach to filling this research lacuna. By formulating a heat balance equation for the thermal - storage ladle baking system, the study embarks on uncharted territory. It will conduct a meticulous comparative analysis of the energy saving effects when the thermal storage ladle baker employs different gas types. An innovative aspect lies in the special focus on analyzing the volumetric heat storage of the ladle lining and shell, an area that has received scant attention in previous studies.

Moreover, the study aims to shed new light on the baking efficiency of different gas types. This innovative research is not only expected to propel the advancement of thermal storage ladle baking technology but also offers novel approaches to enhance the efficiency of the thermal storage ladle system, aligning with the imperatives of energy conservation and high efficiency operation.

2. The establishment of mathematical-physical modelling is of paramount importance

2.1 Fundamental control equations and mathematical models

1) Fundamental control equations

The fundamental control equations employed in this study are as follows [12]:

Continuity equation.

$$\frac{\partial \rho}{\partial t}+\frac{\partial(\rho \mathrm{u})}{\partial \mathrm{x}}+\frac{\partial(\rho \mathrm{v})}{\partial \mathrm{y}}+\frac{\partial(\rho \mathrm{w})}{\partial \mathrm{z}}=0 \tag{1}$$

Energy Conservation Equation.

$$\frac{\partial(\rho T)}{\partial t}+div(\rho uT)=div\left(\frac{k_t}{c_p}gradT\right)+S_T \tag{2}$$

Conservation of momentum equation.

$$\frac{\partial(\rho u)}{\partial t}+div(\rho uu)=div(\mu gradu)-\frac{\partial p}{\partial x}+S_u \tag{3}$$

$$\int \frac{\partial(\rho v)}{\partial t}+div(\rho vu)=div(\mu gradv)-\frac{\partial p}{\partial y}+S_v \tag{4}$$

$$\frac{\partial(\rho w)}{\partial t}+div(\rho wu)=div(\mu gradw)-\frac{\partial p}{\partial z}+S_w \tag{5}$$

In equation (1-5): ρ is density; u, v and w represent the component velocities in the x, y, and z directions, respectively; t is time; T is temperature; K_t is the thermal conductivity of the fluid; C_p is the specific heat capacity; S_T is the heat source term; S_u, S_v, and S_w represent the generalized source terms of momentum, respectively.

2) Turbulence modelling

The standard k-ε model has a mature theoretical basis rooted in turbulent statistical theory. It offers high computational efficiency with only two extra equations. Also, it provides relatively accurate simulation results in high temperature air combustion for various

turbulent flows.
Therefore, the standard k-ε model is employed for turbulent flow in high-temperature air combustion, with the following expression for the transport equation [13, 14] :

Transport equation for turbulent kinetic energy k:

$$\frac{\partial}{\partial t}(\rho k)+\frac{\partial}{\partial x_i}(\rho k u_i)=\frac{\partial}{\partial x_j}\left[\left(\mu+\frac{\mu_t}{\varphi_k}\right)\frac{\partial k}{\partial x_j}\right]+G_k+G_b-\rho\varepsilon-Y_M+S_k \quad (6)$$

The turbulent dissipation rate can be expressed as.

$$\frac{\partial}{\partial t}(\rho\varepsilon)+\frac{\partial}{\partial x_i}(\rho\varepsilon u_i)=\frac{\partial}{\partial x_j}\left[\left(\mu+\frac{\mu_t}{\varphi_\varepsilon}\right)\frac{\partial\varepsilon}{\partial x_j}\right]C_{1\varepsilon}\frac{\varepsilon}{K}(G_k+C_{3\varepsilon}G_b)-C_{2\varepsilon}\rho\frac{\varepsilon^2}{k}+S_\varepsilon \quad (7)$$

The turbulent viscous model can be expressed as.

$$\mu_t=\rho C_\mu\frac{k^2}{\varepsilon} \quad (8)$$

In equation (6-8): p is pressure; k is turbulent kinetic energy; The dissipation rate of k; G_k is the k generation rate generated by the average velocity gradient; G_b is the dissipation rate of k generated by buoyancy; Y_M contributes to the pulsating expansion in compressible turbulence; S_k and S_ε are the source terms for k and ε, respectively; $C_{1\varepsilon}$, $C_{2\varepsilon}$, $C_{3\varepsilon}$ and are the empirical constants; φ_k is the turbulence Plummer's constant of k; and φ_ε is the turbulence Prandt number of ε. Typically, the values of the parameters $C_{1\varepsilon}$, $C_{2\varepsilon}$, $C_{3\varepsilon}$, σ_k and σ_ε are set to 1.44, 1.92, 0.09, 1.0 and 1.3, respectively.

3) Component transport and turbulent combustion model

In this study, non-premixed combustion is employed, with combustion gas and combustion air being injected into the baking zone in a turbulent flow. The net production rate of reaction products can be expressed by the following equation, which utilises a finite rate model for the calculation of the chemical reaction rate of combustion, based on the turbulence chemistry interaction model of the eddy-dissipation model [15, 16].

$$R_{i,r}=v'_{i,r}M_{w,i}A\rho\frac{\varepsilon}{k}\min_{\mathcal{R}}\left(\frac{Y_{\mathcal{R}}}{v'_{\mathcal{R},r}M_{w,\mathcal{R}}}\right) \quad (9)$$

$$R_{i,r}=v'_{i,r}M_{w,i}AB\rho\frac{\varepsilon}{k}\frac{\sum_P Y_P}{\sum_j^N v''_{i,r}M_{w,j}} \quad (10)$$

Equations (9-10) indicate the mass fraction of the product component, reflect the mass fraction of the specific reactant component, and A and B are empirical coefficients, A = 4.0 and B = 0.5.

4) Radiative transfer model

The P-1 model was chosen for the radiative transfer model.

$$\frac{dI(r,s)}{ds}+(a+\sigma_s)I(r,s)=aI_b(r)+\frac{\sigma_s}{4\pi}\int_0^{4\pi}I(r,s')\Phi(s,s')d\Omega' \quad (11)$$

In equation (11), the variables r, s, and s' represent the position vector, direction vector, and scattering direction vector, respectively. σ_s is the scattering coefficient, while $\Omega'$is the steradian angle. The variable a is the absorption coefficient, and I is the radiation intensity, Φ is the phase function.

5) Gas phase combustion modeling

The numerical analysis of the gas phase combustion process employs a mixed fraction-probability density function model [17]. The model has been identified as being particularly suitable for unpressurised turbulent diffusion combustion reactions and has been widely employed in this field. The model treats the combustion problem as a mixed problem using the treatment of solving a single invariant (mixed fraction), and all thermochemical scalars of the combustion process are calculated from the conserved values at the corresponding positions of the flow field.

2.2 Physical model and grid division

As demonstrated in Figure 1, a schematic representation of the ladle dimensions and monitoring points is provided, which is based on an accurate 1:1 geometrical model of a 130t ladle in a steel plant. The ladle's overall height is measured at 3599mm, while the internal height is recorded at 3214mm. The ladle's structural composition consists of a ladle body, a pair of symmetrically arranged burners of equal dimensions, and a ladle cover. The burners are designed with air and fuel inlets of two diameters, 58.45mm and 93.64mm respectively, while the diameter of the air inlet is fixed at 153mm. The flue gases emanating from the combustion process are principally discharged through the burners as the outlets, with a minor efflux of flue gases potentially overflowing from the edge of the ladle.

To facilitate precise monitoring of temperature variations within the ladle, five designated monitoring points, labelled A, B, C, D, and E, have been strategically positioned. Monitoring point A was set at the centre of the working layer at the bottom of the ladle, 0.34m from the bottom; B and C were located on the working layer of the ladle wall 1.39m and 3.39m from the bottom of the ladle, respectively; and D and E were set on the permanent layer of the ladle wall 1.39m and 3.39m from the bottom of the ladle, respectively.

The ladle's overall structure consists of three layers of material, from the exterior to the interior: the shell of the ladle, composed of SM490B with a thickness of 36mm; the permanent layer, constructed from high alumina bricks with a thickness of 85mm; and the working layer, formed from magnesium-carbon bricks with a thickness of 135mm. Despite the uniformity in material composition across the ladle's wall and base, the thicknesses of the constituent layers vary, as delineated in Table 1.

Table 1.
Package wall materials and dimensions

level	work layer	permanent layer	Tundish shell
material	magnesium-carbon brick	high aluminum brick	SM490B
Package wall thickness （mm）	135	85	36
Thickness of the bottom of the bag（mm)	180	130	75
density（kg/m^3）	2900	2380	7830
specific heat capacity（J/kg）	750	857	480
thermal conductivity（W/(mK)）	2.1	1.22	56

2.3 Boundary conditions and operating parameters

Three types of gas, natural gas, coke oven gas and converter gas, which are commonly used as fuels in metallurgical production, were selected for the comparative study, and the specific compositions are shown in Table 2.

Table 2.
Fuel component volume fraction (%)

Type/Composition	natural gas	coke oven gas	converter gas
CO	0.3	9	60.2
CO_2	1	2.3	14.6
H_2	0.7	53.6	1
N_2	4	16.4	18
O_2	0.2	3	0.2
H_2O	-	-	5.7
CH_4	93.8	15.7	-

In order to ascertain the requisite flow rate of three distinct types of fuels in the ladle baking process, it is necessary to calculate the total amount of heat. Given the established correlation between the chemical composition of fuels and the heat produced by combustion, the calorific value of the fuels can be calculated by the law of mixing, as outlined in equation (12).

$$H = H_1 r_1 + H_2 r_2 + H_3 r_3 + \cdots\cdots + H_n r_n \tag{12}$$

In the formula (12): H is expressed as the high calorific value or low calorific value (kJ/Nm^3) of the gas (gas mixture); $H_1, H_2, \cdots H_n$ is the high calorific value or low calorific value (kJ/Nm^3) of each combustible component in the gas; $r_1, r_2, \cdots r_n$ is the volumetric composition of each combustible component in the gas.

The gas calorific formula is expressed as:

$$q = HB\eta \tag{13}$$

In equation (13), the quantity q denotes the heat of the gas (kJ/h). H is the high or low calorific value of the gas in gas mixtures (kJ/Nm^3). η is the combustion efficiency percentage. The equation is calculated according to the idealised combustion efficiency of 100%. B is the gas consumption (Nm^3/h).

$$B = Qt_h \tag{14}$$

In equation (14): Q is the gas flow rate (Nm^3/h); t_h is the baking time (h).

According to the above formula, the inlet flow rates of coke oven gas, natural gas, and converter gas are calculated as follows: B_1=913.73Nm^3/h，B_2=326.17Nm^3/h，B_3=1486.75Nm^3/h。

2.4 Model validation

To validate the accuracy of the numerical simulation results, an experimental platform was built with a similarity ratio of 1:2.5. The dimensions of this setup are specified as follows: the overall height of the ladle measures 1439.6mm, the height of the inner cavity is 1285.6mm, and the diameter of the upper part is 1288 mm. The inner wall of the ladle is composed of the same three layer material used in the numerical simulation, and its thickness is calculated according to the aforementioned similarity ratio. Natural gas was selected as the fuel source, while pure oxygen was used as the combustion gas. The numerical simulation was utilized to identify five monitoring points, which were subsequently connected to thermocouple sensors (as depicted in Fig. 1).

The steel body was initially preheated to 1060K. Subsequently, natural gas at a rate of 130Nm^3/h and oxygen at a rate of 1363Nm^3/h were continuously introduced for non premixed combustion, thus commencing the baking of the steel body. At the end of each 30s reversal cycle, the natural gas and oxygen cylinders connected to the gas pipe on the opposite side of the air inlet were promptly shut off. This was done to prevent any gas leakage. Following this, the two cylinders were reopened to resume the combustion baking process. This cycle was repeated over a total period of 5400s. The purpose of this 5400s baking under optimal conditions was to ensure accurate results. Throughout this process, thermocouple sensors were carefully positioned to monitor the temperature at five specific points. After the baking process was completed, the temperature data was recorded and averaged. This average temperature was then compared with the simulation results. Such a comparison was crucial for ensuring the accuracy and precision of the entire experimental procedure.

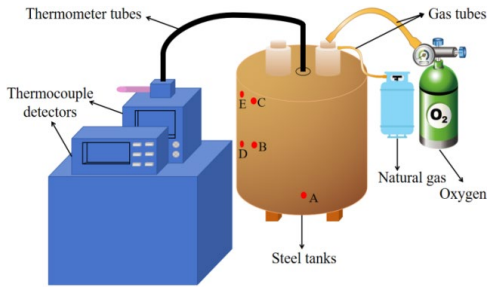

Fig. 1. Schematic diagram of the experimental platform

As depicted in Figure 2, the contrast between the experimental temperature and the simulated temperature at point A is distinct. From the figure, it is apparent that the experimental temperature at point A remains higher than the simulated temperature throughout the entire experimental course. This divergence can be ascribed to the location of point A, which is at the center of the working layer at the bottom of the ladle. As a result, it is more vulnerable to the direct influence of the flame. During the actual baking process, the temperature variation at this point is more intricate and less stable compared to the simulation. This is due to the combined effects of multiple factors. Consequently, the experimental temperature is higher than the simulated temperature. In contrast, for the remaining four monitoring points, the simulated temperature values showed a trend of exceeding the experimental temperature values.

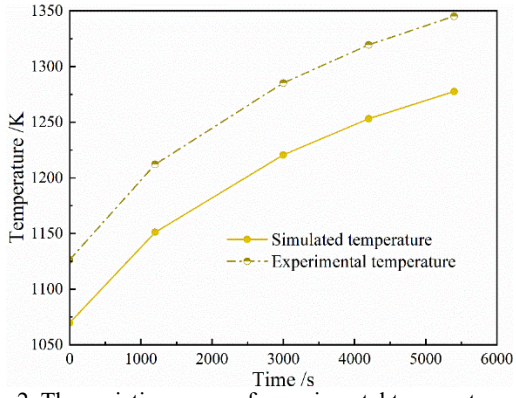

Fig. 2. The variation curve of experimental temperature and simulated temperature at point A

As demonstrated in Figure 3, the variation curves of the experimental temperature at monitoring points B and C are compared with the simulated temperature. As is evident from the figure, the experimental temperatures on the working layer are all lower than the simulated temperatures. The simulation represents an ideal result under specified setup conditions. Discrepancies exist between the air - gas experimental settings and the simulation, with influence from the experimental environment, conditions, and operation process. These factors lead to differences between experimental and simulation results. Although the experimental temperatures at points B and C are lower than the simulated ones, their warming trends during baking are the same, making the results reasonable.

As shown in Figure 4, the experimental and simulated temperature variation curves at monitoring points D and E are presented. The experimental temperatures at these two points are lower than the simulated ones, in line with the results at B and C. The simulated temperature at E is lower than that at some other points. Due to the non uniform influence of flame baking caused by location differences, the experimental simulation error values vary. In Figure 4, the error at E is significantly higher than at D. Still, it's worth noting that the temperature at E has reached the required baking temperature.

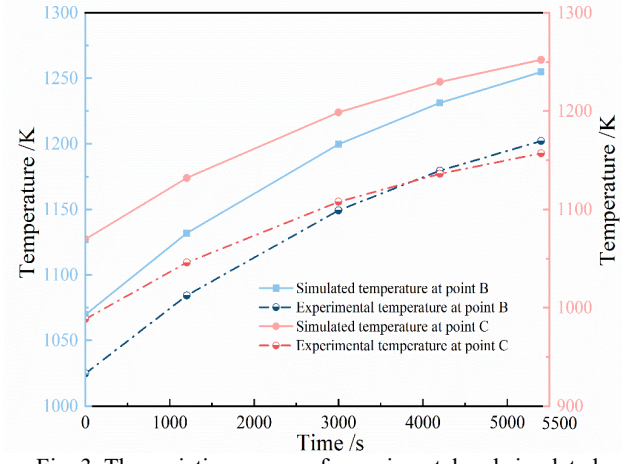

Fig. 3. The variation curves of experimental and simulated temperatures at points B and C

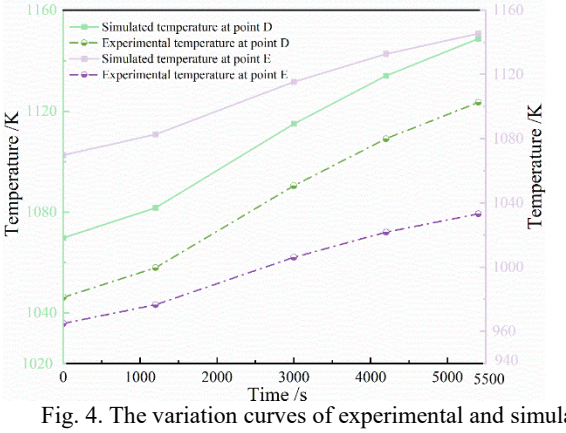

Fig. 4. The variation curves of experimental and simulated temperatures at points D and E

Figure 5 compares the simulated and experimental mean temperatures, along with error results at each monitoring point. The data shows the relative errors between experimental and simulated temperatures at points A, B, C, D, and E are 5.3%, -4.2%, -7.6%, -2.2%, and -9.8% respectively. Notably, there are large temperature differences at points C (84.74K) and E (105.22K), mainly due to their proximity to the flame area and the significant temperature fluctuations from the baking process's switching operation.
Moreover, potential error factors in thermocouple based high temperature measurements must be considered. A comprehensive evaluation shows the identified errors are within acceptable limits.

This validates the model's precision and reliability, laying a solid foundation for future simulation studies.

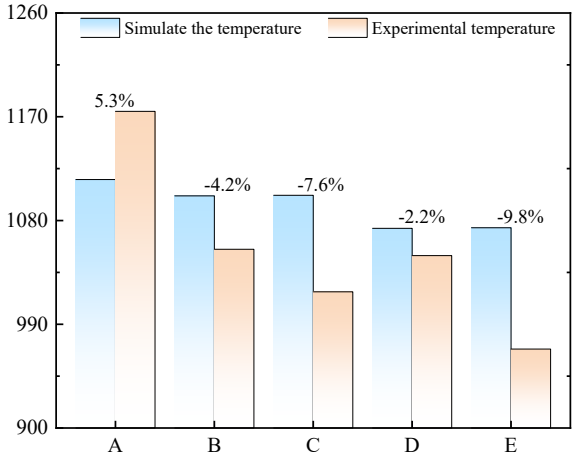

Fig. 5. Comparison of experimental temperature and simulated temperature

3. Heat balance analysis of different gas baking processes

3.1 Heat income analysis

In steel ladle baking, the air is typically introduced at a rate of 15-20m^3/s [18], and an airflow rate of 800m^3/h is more appropriate for the on-site large-scale fire baking stage. In this paper, the injection rate of coke oven gas is specified to be 23.66m/s. The optimal air-fuel ratio for coke oven gas combustion was determined through calculation to be 17.92m/s when the gas is coke oven gas, and the through-flow rate of coke oven gas was calculated to be 913.73Nm^3/h according to Equations 15 and 16.

It is assumed that the total heat released from the three gases is equal, i.e. the chemical heat released from the combustion of the fuels is the same, which is 1.148×10^7kJ/h. Therefore, the sensible heat of the fuels can be neglected.

$$Q = SA \tag{15}$$

Where: Q is the flow rate (Nm^3/h); S indicates the fluid flow rate velocity (m/s); A is the cross-sectional area (m^2).

$$A = \pi r^2 \tag{16}$$

Where: r is the cross-section radius (m).

The calorific values of coke oven gas, natural gas, and converter gas utilised in this study are 1.256×10^4 kJ/Nm^3, 3.519×10^4 kJ/Nm^3, and 7.720×10^4 kJ/Nm^3, respectively. Assuming that the three gases release equal amounts of heat, the total heat released from the coke oven gas after baking for 1.5 hours is kJ. The natural gas and converter gas dosages are 3.262×10^2 Nm^3/h and 1.487×10^2 Nm^3/h, respectively.

Heat release occurs in three main forms: fuel combustion chemical heat, fuel sensible heat, and air sensible heat. Fuel combustion chemical heat, or fuel heat, is the heat from the complete combustion of a unit volume of fuel. Fuel sensible heat, also called fuel heat or combustion calorific value [19,20], is the heat released during fuel combustion. Notably, in this calculation, the fuel's physical sensible heat is excluded.

1) The chemical heat of combustion of fuels.

The achievement of uniformity in the fuel dosage of the three gases is contingent on the precise regulation of their respective fuel inputs.

$$Q_1 = BHt \tag{17}$$

Where:Q_1 is chemical heat of combustion of fuel (kJ); B is amount of fuel (Nm^3/h); H is high or low calorific value of gas (gas mixture) (kJ/Nm^3); t is baking time (h).

The duration of the study was set at 1.5 hours in total. It was imperative that the chemical heat of combustion of the fuels under investigation was uniform, thus ensuring that the three gases were equivalent.

2) Sensible heat of air

In this study, the air was preheated to 1200K, with its initial temperature established at 1069.71K. In other words, the values of tk and tc were set to 1200K and 1069.71K, respectively.

$$Q_2 = B\alpha {L_0}^s(C_k t_k - C_{kc} t_c)t \tag{18}$$

Q_2 is the physical heat brought in by combustion air (kJ); B is the amount of fuel (m^3/h); α is the air coefficient (in industrial equipment, this is generally controlled at 1.05-1.20); ${L_0}^s$ is the theoretical amount of humid air (m3/m3); C_k and C_{kc} is the average specific heat capacity of air between 0-t_k and 0-t_c; t_k is the air temperature (℃); t_c is the ambient temperature (℃).

$${L_0}^s={L_0}^R(1 + 0.00124g_k) \tag{19}$$

${L_0}^s$is moisture content of dry air (q/m3); ${L_0}^R$ is theoretical dry air volume (m3/m3).

$${L_0}^R=0.0238({H_2}^S + {CO_2}^S) + 0.0952{CH_4}^S + 0.0476(m + \frac{n}{4}){C_m H_n}^S + 0.0714{H_2}^S - 0.0476{O_2}^S \tag{20}$$

$$Z^S = Z^g \frac{100}{100+0.124g_m} \tag{21}$$

In Eq. (21): Z^S is volume fraction of any wet component of the gaseous fuel (%); Z^g is corresponding volume fraction of dry component (%); g_m is moisture content of the dry gaseous fuel (g/m^3).

The water content of the three dry gaseous fuels, natural gas, coke oven gas, and converter gas, is 0.27g/m^3, 0.25g/m^3, and 0.30g/m^3, respectively.

The total heat income is hereby defined as follows:

$$\Sigma Q = Q_1 + Q_2 \tag{22}$$

The total heat revenue is calculated using formula 22, and the results are shown in Table 3.

Table 3
Calculation of heat income (kJ)

Gas type	Q_1	Q_2	Q
natural gas	1.722×10^7	9.078×10^6	2.629×10^7
coke oven gas	1.722×10^7	8.080×10^6	2.530×10^7
converter gas	1.722×10^7	6.695×10^6	2.391×10^7

3.2 Heat expenditure analysis

During steel ladle baking, aside from the heat absorbed by the ladle, significant radiant heat loss occurs in the space between the ladle baker and the ladle's edge. Also, heat loss from the ladle's outer wall, heat carried away by water evaporation in the ladle, lining shell heat storage, and heat loss from incomplete fuel combustion are the main heat loss mechanisms in the baking process.

1) Gas sensible heat escaping through the gap between the ladle cover and the ladle edge

The ladle's molten metal is at a high temperature, causing gas to escape with sensible heat. During ladle baking, gases can escape through its gaps due to pressure and temperature differences, serving as a heat loss medium.

$$Q_1' = V_1(C_y t_y - C_{yc} t_c)t \tag{23}$$

In Eq. (23): Q_1' is sensible heat of the gas escaping through the gap between the ladle cover and the ladle rim (kJ); V_1 is the volume of gas escaping through the gap between the ladle cover and the ladle rim (m^3/h); C_y and C_{yc} are average specific heat capacity of the gas escaping through the gap between the ladle cover and the ladle rim between 0-t_y and 0-t_c[$kJ/(m^3 \cdot ℃)$]; t_y is temperature of the escaping gas in the gap between the ladle cover and the ladle rim (℃).

Numerical simulation results show that the escape velocities of natural gas, coke oven gas, and converter gas are 1.74m/s, 2.74m/s, and 2.56m/s respectively. The gas escape volume through the gap between the ladle cover and the ladle edge is calculated by multiplying the escape velocity by the escape area. Figure 7 depicts the three gases escaping along the gap between the ladle cover and ladle, and also shows their sensible heat and heat loss rate .

ξ_i is achieved by the following formula:

$$\xi_i = \frac{Q_i'}{\Sigma Q_i} \times 100\% \tag{24}$$

In Eq. (24):ξ_i is efficiency of each heat loss; Q_i' is each heat expenditure (kJ); ΣQ_i is the sum of each heat expenditure of different gas types.

As shown in Figure 6, the heat loss figure of merit for the three gases can be determined by the area under the curve. Converter gas has the highest value, while natural gas has the lowest. The heat loss rate of the three gases, as they escape through the gap between the ladle cover and the ladle edge, carrying away the gas's sensible heat, are 8.16%, 13.33%, and 23.96% respectively. The loss rate is positively correlated with the heat loss value, and the loss rate of converter gas is more than twice that of natural.

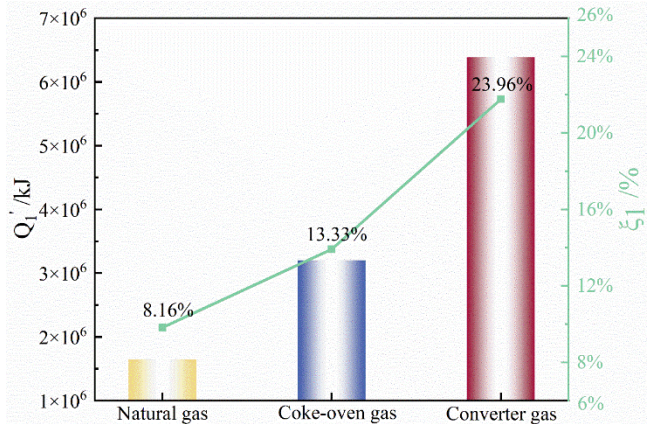

Fig. 6. Comparison of sensible heat of gas escaping from the seam

2) Radiation of heat through the gap between the ladle cover and the ladle edge

The radiant heat in the gap between the ladle lid and the ladle rim (Q_2') represents a complex physical phenomenon encompassing both heat conduction and radiation processes. Within the realm of steel smelting, the design and operational parameters of the ladle exert a profound influence on the dissipation and transfer of heat. Equation (25) provides a convenient means for calculating this heat loss.

$$Q_2' = 20.41 A_y \emptyset \tau \left[\left(\frac{273+t_y}{100}\right)^4 - \left(\frac{273+t_c}{100}\right)^4\right] t \tag{25}$$

Where A_y is the escaping area along the gap between the ladle cover and the ladle; $\emptyset$ is the angular coefficient (in this paper, $\emptyset$ is taken as 0.5); τ is the time when the ladle cover is open (i.e., the time the gap exists).

As depicted in Figure 7, a comparison is presented for the radiant heat of the three gases passing through the gap between the ladle cover and the ladle rim, along with their respective heat loss rate. The results indicate that the radiative heat loss rate of these gases are 8.35%, 8.68%, and 14.62% respectively. Significantly, although the radiant heat values of natural gas and coke oven gas are equal, the heat loss rate of coke oven gas is higher than that of natural gas. In contrast, converter gas exhibits a higher heat loss rate compared to the other two gases.

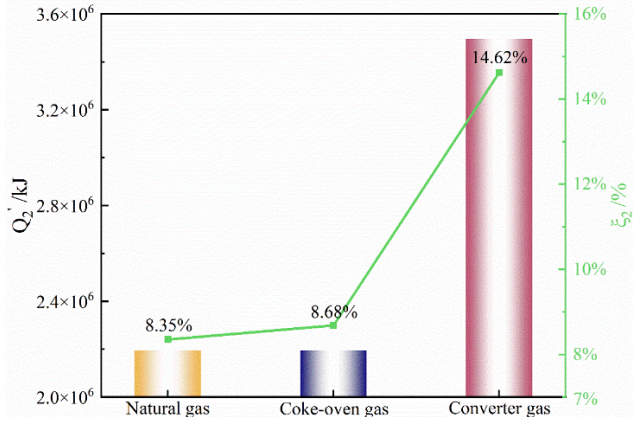

Fig. 7. Comparison of radiant heat from gaps

3) Chemical heat of gas through the gap between the ladle cover and the ladle edge

The chemical heat of gases escaping through the gap between the ladle lid and the ladle rim (Q_3') represents a crucial thermodynamic phenomenon, especially in the domains of steel smelting and metal casting operations. During the smelting process, the high temperature conditions within the ladle trigger chemical reactions that generate gases such as CO, CO_2, and H_2O. These gases carry substantial chemical heat at elevated temperatures. The chemical heat of these gases mainly stems from the conversion of chemical energy into thermal energy during the transformation of reactants. Equation (26) can be utilized to calculate this loss.

$$Q_3' = V_1(126CO + 108H_2 + 358CH_4 + 589C_mH_n)t \quad (26)$$

As shown in Figure 8, a comparison is made of the chemical heat loss of the gas escaping through the gap between the ladle cover and the ladle rim for the three gases, along with their respective heat loss rate. The chemical heat loss rate of the gas escaping through this gap for the three gases are 4.27%, 3.75%, and 1.79% respectively. In contrast to the trends noted in several previous heat expenditure studies, both the heat expenditure and the heat loss rate are highest for natural gas and lowest for converter gas.

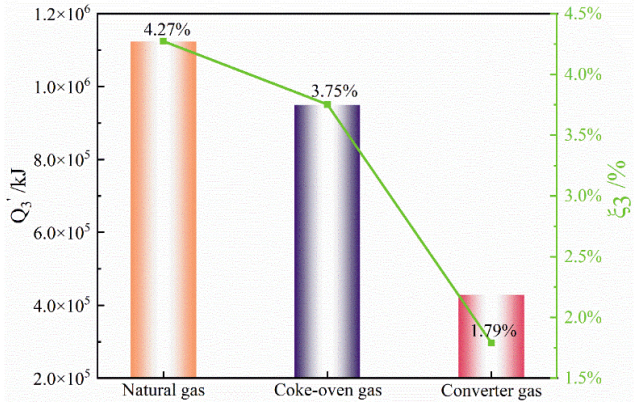

Fig. 8. Comparison of chemical heat of gas escaping from the seam

4) Heat dissipation on the outer surface of the ladle and ladle cover

In the smelting process, heat dissipation from the exterior surfaces of the ladle and ladle cover (Q_4') is a crucial thermal management issue. This involves multiple heat transfer mechanisms: conduction, convection, and radiation. Heat conduction refers to the transfer of heat from the interior to the exterior of the ladle and ladle cover materials via conductive pathways within the materials. Convection, conversely, is the heat exchange between the external environment and the ladle surface. The movement of air around the ladle carries away heat from the surface, causing convective heat dissipation. Radiation, lastly, is the release of heat from a high - temperature surface to its surroundings, a process that becomes increasingly significant at elevated temperatures. Equation (27) can be used to calculate this component of heat loss.

$$Q_4' = \Sigma q_i A_i t \quad (27)$$

Where A_i is area of heat dissipation from the outer surface of part i (m^2); q_i is average area heat flux from the outer surface of part i [kJ/(m^2·h)].

From the post processing of the numerical simulation (Fig. 9), it is clear that the external surface heat dissipation areas of all three gases are equal, and the average external surface area heat fluxes of natural gas, coke oven gas, and converter gas can be derived. The data shows that the heat dissipation on the outer surfaces of the ladle and ladle cover is negatively correlated with their heat loss rate. The heat dissipation values on the outer surfaces of the ladle and ladle cover for the three gases are 9.391×10^5kJ, 9.389×10^5kJ and 9.377×10^5kJ respectively. Evidently, natural gas has the highest heat dissipation. And the corresponding heat loss rate are 3.57%, 3.71%, and 3.92%, respectively. Therefore, although natural gas shows the highest heat dissipation on the outer surfaces of the ladle and ladle cover, it has the lowest heat loss efficiency. Conversely, converter gas shows the opposite trend, with the highest heat loss rate.

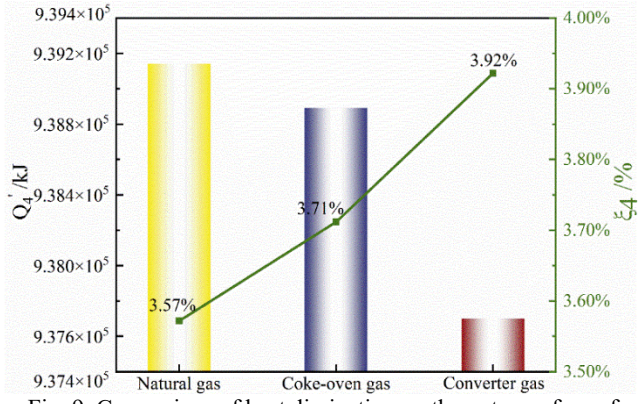

Fig. 9. Comparison of heat dissipation on the outer surface of ladle and lid

5) Heat storage of steel ladle lining and outer shell

The specific heat capacity and thermal conductivity of the materials used in the lining and shell directly influence their heat storage capacity. Additionally, the shape and size of the ladle impact its overall heat holding capacity. It can be inferred that the

larger the ladle's volume, the greater its heat storage capacity. Moreover, the temperature differential between the inner and outer parts of the ladle lining and shell affects heat transfer and heat storage efficiency. Equation (28) can be used to calculate the heat expenditure of this part

$$Q_5' = \Sigma m_i c_i (t_w - t_0) \tag{28}$$

Where Q_5' is heat storage of ladle lining and shell (kJ); m_i is a mass of each material of ladle lining and shell (kg); c_i is specific heat capacity of each material of ladle lining and shell [kJ/(m³℃)]; t_w is the average temperature of the inner and outer walls of the steel bag lining and shell at the end of baking process; $t_0$is the average temperature of the inner and outer walls of the ladle lining and shell at the beginning of the baking process (℃).

Since the temperature of each gas changes over the course of the baking process, the average temperatures of the inner and outer walls of the ladle liners and shells at the start and end of the baking process differ. As depicted in Figure 10, the three types of gas show distinct variations during the baking process. It is evident that in the initial stage of baking, the values of the three gases are nearly the same. However, after approximately 1000s of baking, the heat storage value of the converter gas in the ladle lining and outer shell gradually increases, while those of natural gas and coke oven gas rise rapidly. At 3000s of baking, the curves of natural gas and coke oven gas diverge, with natural gas showing a steeper growth rate.

By the end of the baking period, the heat storage in the ladle lining and outer shell of natural gas reaches 8.290×10⁶kJ, while that of coke oven gas and converter gas is 7.868×10⁶kJ and 6.064×10⁶kJ respectively. Consequently, the final heat storage of natural gas is 5.37% higher than that of coke oven gas and 36.72% higher than that of converter gas. A comparison of the results shows that natural gas has superior heat storage capabilities compared to the other two gases at all time points.

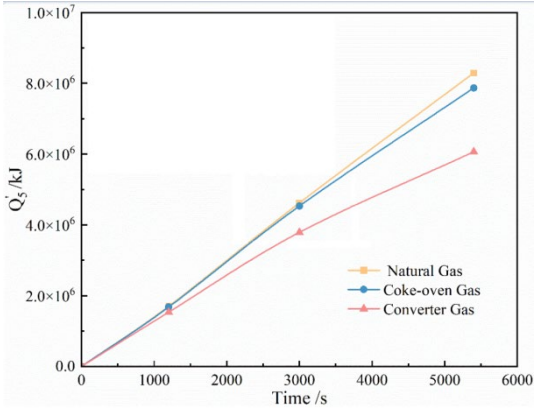

Fig. 10. Variation curve of with time for graphical illustration

6) Heat storage of steel ladle cover

The heat storage of steel ladle cover (Q_6') can be calculated by Equation 29

$$Q_6' = m_j c_j (t_g - t_1) \tag{29}$$

Where m_j is mass of the cover (kg); $c_j$is specific heat capacity of the cover; t_g is average temperature of the inner and outer walls at the end of the baking of the cover; t_1 is the cover temperature at the beginning of baking; t_g is the cover temperature at the end of baking

Figure 11 showcases comparative bar graphs of the heat storage in the ladle cover for the three gases, accompanied by the corresponding schematic diagrams of the heat loss rate. From this figure, the variation in heat storage is clearly visible. Evidently, natural gas exhibits the highest heat accumulation in the ladle lid and the highest heat loss efficiency in lid accumulation, while converter gas has the lowest values for these two parameters. Notably, the Q_6' values for natural gas and coke oven gas are relatively close, but the values for converter gas are significantly lower than those of the other two gases.

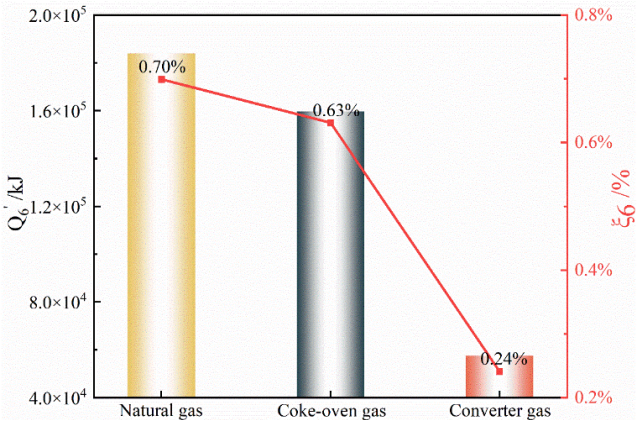

Fig. 11. Comparison of heat accumulation in the capsule

7) Sensible heat carried away by exhaust gas

During the ladle baking process, a substantial amount of sensible heat is transferred from the flue gases generated by fuel combustion. This transfer of sensible heat causes an energy loss within the system, thereby decreasing its overall efficiency. Equation (30) can be used to calculate this specific heat loss.

$$Q_7' = (B\beta V_n^S - V_1)(C_{y2}t_{y2} - C_{yc}t_{yc})t \tag{30}$$

In the formula (30), Q_7' is the sensible heat carried away by exhaust gas (kJ); β is incomplete combustion flue gas correction coefficient (this reserach takes 0.95); C_{y2} and C_{yc} are the average specific heat capacity of flue gas between 0-t_{y2} and 0-t_{yc}[kJ/(m³ · ℃)]; t_{y2} is flue gas out of the heat storage room of the exhaust temperature (℃); $V_n{}^S$is the actual wet flue gas volume at complete combustion (m^3/m^3).

$$V_n^S = V_0 + [\alpha(1 + 0.00124g_k) - 1]L_0^g \tag{31}$$

$$V_0 = 0.01\left[CO^S + 3CH_4^S + \left(m + \frac{n}{2}\right)C_mH_n^S + CO_2^S + H_2^S + 2H_2S^S + N_2^S + H_2O^S\right] + 0.79L_0^g \tag{32}$$

Where V_0 is theoretical flue gas volume.

The sensible heat values of the external flue gas take away for

natural gas, coke oven gas and converter gas have been calculated and are found to be 1.204×10^{7}kJ, 6.814×10^{6}kJ and 7.591×10^{6}kJ, respectively. These values correspond to heat loss rate of 47.17%, 42.07%, and 31.67%, respectively. In this analysis, natural gas has the highest Q_7' and converter gas has the lowest. Furthermore, the amount of sensible heat carried away by natural gas and coke oven gas outgassing flue gas accounted for a larger share of the sum of the heat losses of these two gases, and their loss rates in terms of the amount of sensible heat carried away by the outgassing flue gas were close to half.

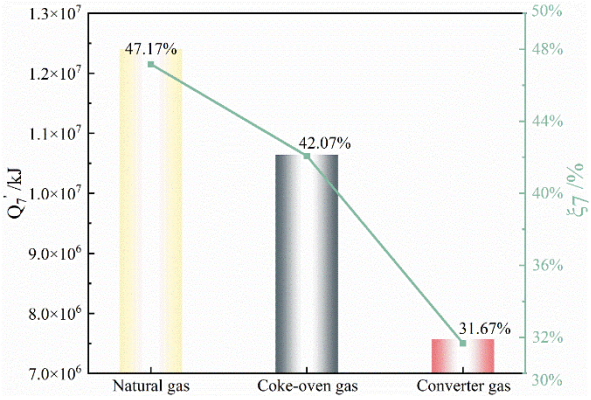

Fig. 12. Comparison of sensible heat carried away by external flue gas

8) Calculation of total heat expenditure

The total heat expenditure can be calculated using formula 33.

$$\Sigma Q' = Q_1' + Q_2' + Q_3' + Q_4' + Q_5' + Q_6' + Q_7' \tag{33}$$

As depicted in Figure 13, a histogram showcases the percentage of total heat expenditure for natural gas, coke oven gas, and converter gas. From the figure, it is clear that for each gas type, the sensible heat carried by the outgoing flue gas accounts for the largest percentage. In contrast, the heat accumulated in the ladle cover represents the smallest percentage in all cases, with all values being less than 1%. Additionally, the chemical heat of the gas escaping through the gap between the ladle cover and the ladle rim, along with the heat dissipated from the outer surfaces of the ladle and the ladle cover, each contribute no more than 5% of the total heat.

The chemical heat of the three gases escaping through the gap between the ladle cover and the ladle rim does not vary substantially. The proportion for natural gas and coke oven gas is approximately 28%, while for converter gas, it is 23.80%, which is only around 4.0% lower than the other two gases. The heat accumulated in the ladle cover of natural gas and coke oven gas, as well as the sensible heat carried out by the flue gas, is lower compared to that of converter gas. Moreover, the proportion of these two types of heat expenditure for converter gas is more than 15% higher.

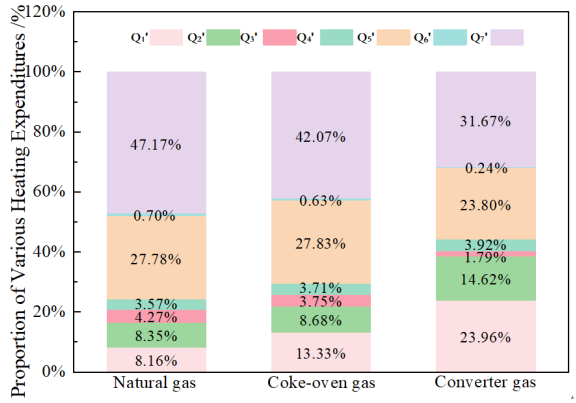

Fig. 13. Proportion of individual heat expenditures to total heat expenditures

3.3 Heat efficiency of steel ladle baking with different gas types

The baking thermal efficiencies of different gas types were calculated by Equation (34).

$$\eta = \frac{Q5'}{\Sigma Q} * 100\% \tag{34}$$

Where η is the thermal efficiency of heat storage ladle baking system (%).

As evident from Figure 14, when the chemical heat of fuel is controlled at the same level, the volumetric heat storage value and the total heat income of the natural gas baked steel ladle lining and shell are the highest, whereas those of the converter gas baked ones are the lowest. Commonly, the higher the calorific value of the fuel, the more heat is produced upon combustion, resulting in a higher thermal efficiency. Only by controlling the heat quantity to be the same can we determine which gas is of the highest quality fuel. By calculating the average values of various heat expenditures and heat revenues at different time points, the average baking thermal efficiencies of natural gas, coke oven gas, and converter gas throughout the entire baking process are found to be 27.78%, 27.83%, and 23.80% respectively.

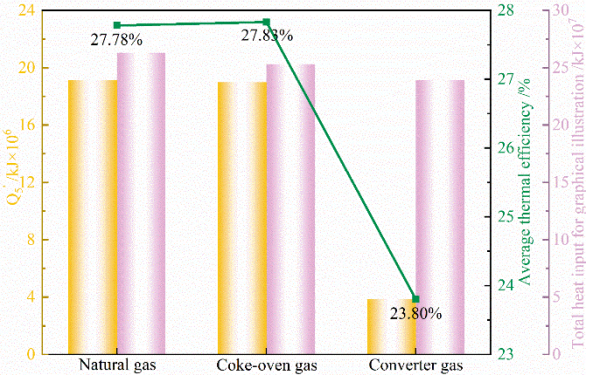

Fig. 14. Comparison of baking thermal efficiency

4. Conclusions

1) For each type of gas, the outgoing flue gas conveys the largest amount of sensible heat, while the heat stored in the ladle cover represents the smallest proportion, accounting for less than 1%. The chemical heat of the gases escaping through the gap between the ladle cover and the ladle rim, along with the heat dissipated from the outer surfaces of the ladle and its cover, does not exceed 5% of the total heat.
2) During the baking processes of natural gas, coke - oven gas, and converter gas, the heat loss rates of the sensible heat of gases escaping through the gaps were 8.16%, 13.33%, and 23.96% respectively, and the radiant heat loss rates through the gaps were 8.35%, 8.68%, and 14.62% respectively.
3) In the initial stage of roasting, the roasting thermal efficiencies of the three gases showed little variation. After one and a half hours of baking, the average thermal efficiency of the thermal storage baking system for natural gas, coke oven gas, and converter gas was determined to be 27.78%, 27.83%, and 23.80% respectively.

Acknowledgments

The authors are grateful for the financial support by Innovation and Entrepreneurship Training Program for College Students and Project of Liaoning Provincial Department of Education (JYTMS20230932).

References

[1] Zhang, H., Zhou, P. & Yuan, F. (2021). Effects of ladle lid or online preheating on heat preservation of ladle linings and temperature drop of molten steel. *Energy*. 214, 118896, 1-11. DOI: 10.1016/j.energy.2020.118896.
[2] Chen, C-H. & Ronney, P.D. (2011). Three - dimensional effects in counterflow heat - recirculating combustors. *Proceedings of the Combustion Institute*. 33(2), 3285-3291. https://doi.org/10.1016/j.proci.2010.06.081.
[3] Li, G., Liu, J., Jiang, G. & Liu, H. (2015). Numerical simulation of temperature field and thermal stress field in the new type of ladle with the nanometer adiabatic material. *Advances in Mechanical Engineering*. 7(4), 1-13. https://doi.org/10.1177/1687814015575988.
[4] Nemitallah, M.A., Habib, M.A., Badr, H.M., Said, S.A., Jamal, A., Ben-Mansour, R., Mokheimer, E.M.A. & Mezghani, K. (2017). Oxy-fuel combustion technology: current status, applications, and trends. *International Journal of Energy Research*. 41(12), 1670-1708. https://doi.org/10.1002/er.3722.
[5] Schaffel-Mancini, N., Mancini, M., Szlek, A. & Weber, R. (2010). Novel conceptual design of a supercritical pulverized coal boiler utilizing high - temperature air combustion (HTAC) technology. *Energy*. 35(7), 2752-2760. https://doi.org/10.1016/j.energy.2010.02.014.
[6] Suda, T., Takafuji, M., Hirata, T., Yoshino, M. & Sato, J. (2002). A study of combustion behavior of pulverized coal in high - temperature air. *Proceedings of the Combustion Institute*. 29(1), 503-509. https://doi.org/10.1016/S1540-7489(02)80065-7.
[7] Weber, R., Gupta, A.K. & Mochida, S. (2020). High - temperature air combustion (HiTAC): how it all started for applications in industrial furnaces and prospects. *Applied energy*. 278, 115551. DOI: 10.1016/j.apenergy.2020.115551.
[8] Weber, R., Smart, J.P., vd Kamp, W. (2005). On the (MILD) combustion of gaseous, liquid, and solid fuels in high temperature preheated air. *Proceedings of the combustion institute*. 30(2), 2623-2629. https://doi.org/10.1016/j.proci.2004.08.101.
[9] Weihong, Y. & Blasiak, W. (2004). Combustion performance and numerical simulation of a high - temperature air - LPG flame on a regenerative burner. *Scandinavian Journal of Metallurgy*. 33, 113-120. https://doi.org/10.1111/j.1600-0692.2004.00675.x.
[10] Lille, S., Blasiak, W., Mo¨ rtberg, M., Dobski, T. & Yang, W. (2002). Heat Flux Evaluation in a Test Furnace Equipped With High - Temperature Air Combustion (HTAC) Technique[C]. In International Joint Power Generation Conference, 24-26 June 2002 (pp.643 – 649). Scottsdale, Arizona, USA.
[11] Sánchez, M., Cadavid, F. & Amell, A. (2013). Experimental evaluation of a 20 kW oxygen - enhanced self - regenerative burner operated in flameless combustion mode. *Applied Energy*. 111, 240 - 246. https://doi.org/10.1016/j.apenergy.2013.05.009.
[12] Haworth, D.C. (2010). Progress in probability density function methods for turbulent reacting flows. *Progress in Energy and Combustion Science*. 36(2), 168-259. https://doi.org/10.1016/j.pecs.2009.09.003.
[13] Ma, L., Naud, B. & Roekaerts, D. (2016). Transported PDF modeling of ethanol spray in hot - diluted coflow flame. *Flow, Turbulence, and Combustion*. 96, 469-502. https://doi.org/10.1007/s10494-015-9623-3.
[14] Lygidakis, G.N. & Nikolos, I.K. (2012). Using the finite - volume method and hybrid unstructured meshes to compute radiative heat transfer in 3-D geometries. *Numerical Heat Transfer, Part B: Fundamentals*. 62, 289-314. https://doi.org/10.1080/10407790.2012.707012.
[15] Moradi, J., Gharehghani, A. & Mirsalim, M. (2020). Numerical investigation on the effect of oxygen in combustion characteristics and to extend low load operating range of a natural-gas HCCI engine. *Applied Energy.* 276, 115516, 1-14. DOI:10.1016/j.apenergy.2020.115516.
[16] Hosseini, A. A., Ghodrat, M., Moghiman, M. & Pourhoseini, S. H. (2020). Numerical study of inlet air swirl intensity effect of a Methane - Air Diffusion Flame on its combustion characteristics. *Case Studies in Thermal Engineering*. 18, 100610. https://doi.org/10.1016/j.csite.2020.100610.
[17] Wang, S., Wen, Z., Dou, R., Xiao, Y., Guan, Y. & Liu, X. (2022). Numerical study on the mixing process of hot desulfurization slag and converter steel slag. *Case Studies in Thermal Engineering*. 40, 102561, 1-13. https://doi.org/10.1016/j.csite.2022.102561.
[18] Qi, F., Shan, J., Li, B. & Baleta, J.. (2020). Numerical study on ladle baking process of oxy - fuel combustion. *Thermal*

Science. 24, 3511-3520. https://doi.org/10.2298/TSCI200318272Q.

[19] Su, F., Fang, L., Kang, Z. & Zhu, H. (2023). Numerical simulation om heat transfer of multi - layer ladle in empty and heavy condition. *Frontiers in Heat and Mass Transfer*. 20(1), 1-9. DOI:10.5098/hmt.20.14.

Hou, A., Jin, S., Harmuth, H. & Gruber, D. (2018). A method for steel ladle lining optimization applying thermomechanical modeling and taguchi approaches. *The Journal of The Minerals, Metals & Materials Society (TMS).* 70, 2449-2456. https://doi.org/10.1007/s11837-018-3063-1